Materials Science in Semiconductor Processing xxx (xxxx) xxx

Contents lists available at ScienceDirect

Materials Science in Semiconductor Processing

journal homepage: http://www.elsevier.com/locate/mssp

Current-voltage characteristics of iron-implanted silicon based Schottky diodes

J.O. Bodunrin, D.A. Oeba, S.J. Moloi *

Department of Physics, College of Science, Engineering and Technology, University of South Africa, Private Bag X6, Florida, 1710, South Africa

ARTICLE INFO

Keywords:
Silicon
Diode
Ohmic I–V
Radiation detectors

ABSTRACT

Current-voltage (*I–V*) measurements were carried out on undoped and iron (Fe) doped *n*-silicon (*n*-Si) to establish and study a change in electrical properties of the material-based diodes with Fe doping concentration. Fe doping was achieved by implantation at the energy of 160 keV to fluences of 10^{15}, 10^{16} and 10^{17} ion/cm^2. The obtained results indicated that the diodes were well fabricated and Fe doping resulted in a diode behaviour changing from normal exponential to ohmic *I–V* behaviour. This ohmic behaviour was explained in terms of Fe-induced defect levels that were positioned at the centre of the energy gap. An *I–V* ohmic region increased with fluence indicating that the density of defect levels has increased with Fe implantation fluence. A change in diode conduction mechanism domination and parameters with fluence were investigated. The obtained *I–V* properties of Fe doped Si-based diodes were similar to those of the diodes that were fabricated on radiation-hard materials indicating that Fe, too, is a promising dopant in a quest to improve radiation-hardness of Si to be used in high energy physics experiments.

1. Introduction

Crystalline silicon is used for fabrication of radiation detectors in high energy physics experiments due to its unique advantages like moderate energy gap, stability in high temperature and cost-friendly due to its abundance in nature, to mention the few. Detectors that are made from this material, however, gets damaged by the same radiation they intend to detect. The damage results in defect levels in the energy gap of Si that are responsible for a change in the microscopic properties of detectors. It is therefore important that radiation-hardness of Si is improved to make the material suitable for the fabrication of efficient radiation detector to be used in the current and future high energy physics experiments [1].

In trying to improve radiation-hardness of the material, numerous studies have shown that a heavy pre-irradiation [2] oxygenation [3] and doping Si with metals such as gold (Au) and platinum (Pt) [4] are promising methods. In Si, Au and Pt were found to be responsible for relaxation behaviour of the material [5] but they are, however, relatively expensive resulting in very limited research on radiation-hardness of Si. It is, therefore, important that the effects of other metal dopants in Si are established and studied. These dopants should be abundant and have similar behaviour as Au and Pt in Si.

In *p*-Si, Fe acts as donor impurity consequently reducing the concentration of holes [6], hence, reducing the conductivity of the material. The resistivity of *n*-Si, on the other hand, has been found to remain unchanged after doping with Fe concentration of 10^{14} cm^{-3} [7]. Based on the literature reviewed, the effects of Fe on electrical properties of Si at a concentration higher than 10^{14} cm^{-3} have not been studied. In Si, Fe creates defect levels at E_V +0.40, E_C -0.55 and E_C -0.27 eV in the energy gap [8]. The main motive of studying the effects of Fe dopants in Si is due to ~0.55 eV defect level, which was found to be induced by Au and Pt [9,10]. A defect level at ~0.56 eV in the energy gap is responsible for relaxation behaviour of Si [11]. Devices fabricated on relaxation material show ohmic *I–V* behaviour [5,11] and they have been proven to be resistant to radiation damage [12]. These devices, however, have high leakage current showing that their radiation detection sensitivity is low. This shortfall encourages a search of the most suitable dopant to improve Si properties for radiation detection applications.

In this work, diodes were characterized using *I–V* technique to investigate the effects of Fe doping on the electrical properties of Si-based devices. The results indicate, for the first time, that in Si, Fe exhibits similar properties as other metals (Au and Pt) that have been found promising to improve radiation-hardness of Si. Hence, Fe could be a suitable replacement in case these two metals are disqualified due to

* Corresponding author.
E-mail address: moloisj@unisa.ac.za (S.J. Moloi).

https://doi.org/10.1016/j.mssp.2020.105524
Received 24 April 2020; Received in revised form 6 September 2020; Accepted 20 October 2020

their unavailability and scarcity.

2. Experimental procedure

2.1. Material preparation

In this study, an *n*-Si wafer polished on one side was diced into 0.9 cm × 0.9 cm square substrates. The resistivity of the material was quoted ranging from 1 to 20 Ω-cm with a thickness of 275 ± 25.0 μm. The standard cleaning procedure using methanol, acetone, trichloroethane and de-ionized water was used [5,13] to remove any handling grease and residue. An oxide layer was removed by dipping the substrates into 40% hydrofluoric (HF) solution. The substrates were then blow-dried using nitrogen gas before loading into a high-vacuum chamber for implantation. The substrates that were mounted on holders labelled A15, B16 and C17 were implanted with 160 keV using the Varian-Extrion 200-20A2F ion implanter at iThemba LABS (Gauteng), South Africa to the fluences of 10^{15},10^{16} and 10^{17} ion/cm^2, respectively. Pieces that were not implanted were labelled unimplanted *n*-Si.

Transport of Ions into Matter (TRIM) simulations were used to predict the distribution of Fe in Si for 160 keV prior to implantation. A theoretical profile of Fe implanted at an energy of 160 keV shown in Fig. 1 predicts a projected range of ~ 134 nm with a maximum implantation depth of ~ 280 nm for the highest fluence. Fig. 1 predicts that the damage due to Fe implantation is up to the depth of ~ 280 nm. This damage is due to the collision of Fe with Si atoms and it increases with fluence. Due to this collision the host atoms are being displaced resulting in the creation of vacancies and interstitials, defects in Si bulk. As Fe penetrates in Si, it loses its energy due to atomic nuclear and electron cloud interactions.

2.2. Diode fabrication

Schottky diodes were fabricated on unimplanted and Fe -implanted crystalline *n*- Si. Prior to diode fabrication, Si pieces were cleaned again using the similar procedure as described in Refs. [5,13]. The pieces were then loaded into an evaporation chamber for the formation of Schottky contacts. The contacts were achieved by evaporation and deposition of 100 nm Au through a mask of 0.6 mm diameter holes at room temperature. The deposition was carried at 10^{-6} mbar at the rate of 1 Å/s. The Ohmic contact was then realized by evaporation and deposition of Al onto the back (unpolished) surface of the pieces. The finished devices each consists of 6 diodes on a piece and with one common ohmic contact. It has been reported that an oxygen layer of 1–3 nm thick would always be found on the surface even after etching Si wafers with HF solution [14]. The effects of the layer on the diode properties are, therefore, assumed common to all the diodes since they were fabricated in the same conditions.

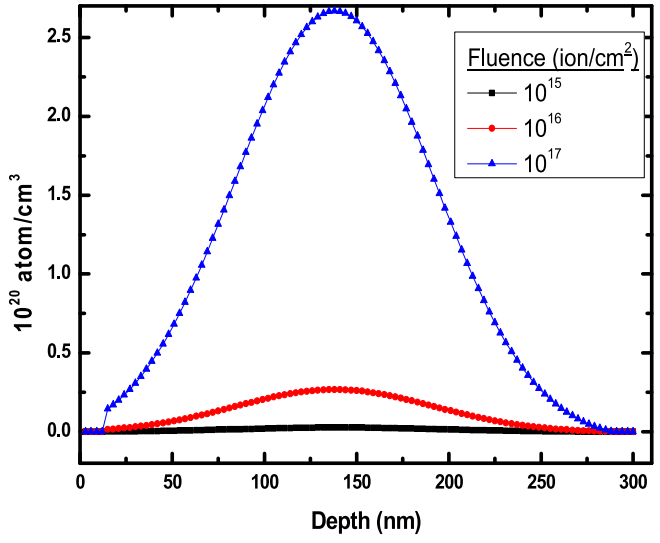

Fig. 1. TRIM simulations for Fe implantation into Si with different fluences.

2.3. Device characterization

Devices are Schottky diodes that were fabricated on unimplanted and Fe-implanted *n*-Si using Au and Al for Schottky and ohmic contacts, respectively. The diodes were characterized by *I–V* technique using Keithley 6487 picoammeter with a voltage source. The measurements were taken with the devices placed in the dark and at room temperature (303 K). The temperature was closely monitored for every sample under test before, during and after carrying out the measurements.

3. Results and discussion

The *I–V* trends for each diode in this work are represented in different scales to investigate the quality of the fabricated device and to study a variation of device current trends as a function of Fe fluence implanted in Si. Fig. 2(a) shows *I–V* characteristics of the unimplanted *n*-Si-based diode in a linear-linear scale. As expected, the current is completely independent of voltage in this scale since the reverse current is due to minority carriers (holes) in *n*-Si. In forward bias, the current remains independent of voltage till ~0.4 V since the electrons have not gained enough energy to surmount the junction barrier. At voltages higher than ~ 0.41 V, the current increases exponentially indicating that as they diffuse in the depletion region, the high charge carrier density is withdrawn to the opposite electrodes contributing to the measured current. This is a typical behaviour of a semiconductor device and it indicates that the diodes were well fabricated [15–17].

Fig. 2(a) obeys a well-known semiconductor diode equation [15–17],

$$I = I_S\left[\exp\left(\frac{eV}{\eta kT} - 1\right)\right] \quad (1)$$

where I_S is the saturation current, e is the electronic charge, V is the applied voltage, η is the ideality factor, k is the Boltzmann's constant and T is the temperature.

Fig. 2(b) shows *I–V* characteristics of unimplanted *n*-Si-based diode in the logarithmic scale. A reverse current trend shows three linear regions with different slopes of 0.98, 2.09 and 0.09 at voltages ranging from 0 V to 0.1 V for region i, 0.1 V–0.32 V for region ii and 0.34 V–2 V for region iii, respectively. The slope for the first region (i) is close to unity indicating that the current increases linearly with voltage while the intermediate region (ii) indicates that the current increases exponentially with voltage in this scale. A very low slope in the last region indicates that the device gets fully depleted at 0.31 V, hence the current saturates. The saturation of the current means that after this voltage, there are no additional charge carriers withdrawn from the space charge region to opposite electrodes, hence the region has attained its full depletion width.

A forward current trend shows three linear regions (i, ii and iii) with slopes of 1.6, 5.4 and 2.7, respectively in Fig. 2 (b) indicating that there are different conduction mechanisms involved in this device. A low slope in the first region indicates that the current increases gently with voltage due to the electric field injected carrier density being lower than the thermal generated carrier density. A high slope evaluated in intermediate voltage range possibly indicates that the dominant conduction mechanism in device is space-charge-limited current [18,19]. In this region the electric injected carrier density is much higher than the thermal carrier density. The slope of the last region is lower because of the series resistance, R_S, making equation (1) to be approximated as $I = I_S\left[\exp\left(\frac{eV-IR_S}{\eta kT}\right)\right]$ at high voltages. Similar results have been reported by

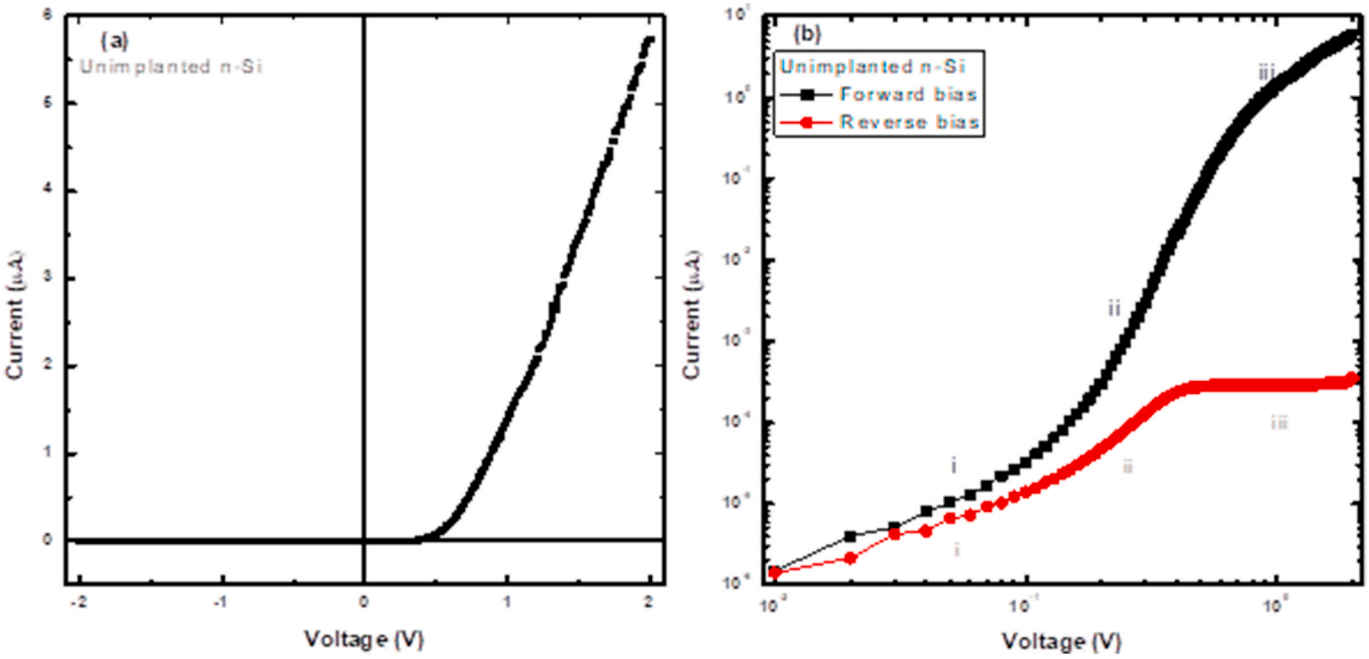

Fig. 2. I–V characteristics of the diode fabricated on un-implanted n-Si in linear-linear (a) and in logarithmic (b) scales.

other authors before with the forward current trend higher than the reverse current trend indicating that charge carrier distribution in the material is mainly due to recombination mechanism [17,19]. The results presented in Fig. 2 are similar to those presented before [19,20] confirming that the diode was well fabricated.

Fig. 3(a) shows *I–V* characteristics of the diode fabricated on Si implanted by Fe to a fluence of 10^{15} ion/cm^2. Unlike in the case of the unimplanted *n*-Si-based diode in Fig. 2(a), the reverse current in Fig. 3 (a) varies with voltage indicating that Fe-induced defects are responsible for the generation of minority carriers increasing the reverse current. Due to this increase in high charge carrier density, the linear region of reverse current is extended to forward bias up to 0.3 V. At the voltages higher than 0.31 V, the forward current increases rapidly with voltage.

In trying to understand the effects of Fe-doping on the *I–V* trends, the plots of Fig. 3(a) were plotted in the logarithmic scale shown in Fig. 3(b). The reverse current trend does not show any tendency of saturation as the current increases linearly with voltage for the whole voltage range. At low voltage range (0.01–0.31 V), the forward and reverse currents are the same indicating that the rate of charge carrier generation (g) is the same as that of charge recombination (r). $g = r$ if charge distribution in the material is dominated by defect levels at the centre of the energy gap [11]. These defects are *g-r* centres that interact with both bands and are responsible for a change in material from lifetime to relaxation behaviour [21]. Relaxation material is radiation-hard since the effects of radiation have been found suppressed [12]. In relaxation material, the Fermi energy is pinned at the intrinsic-position and it has been found

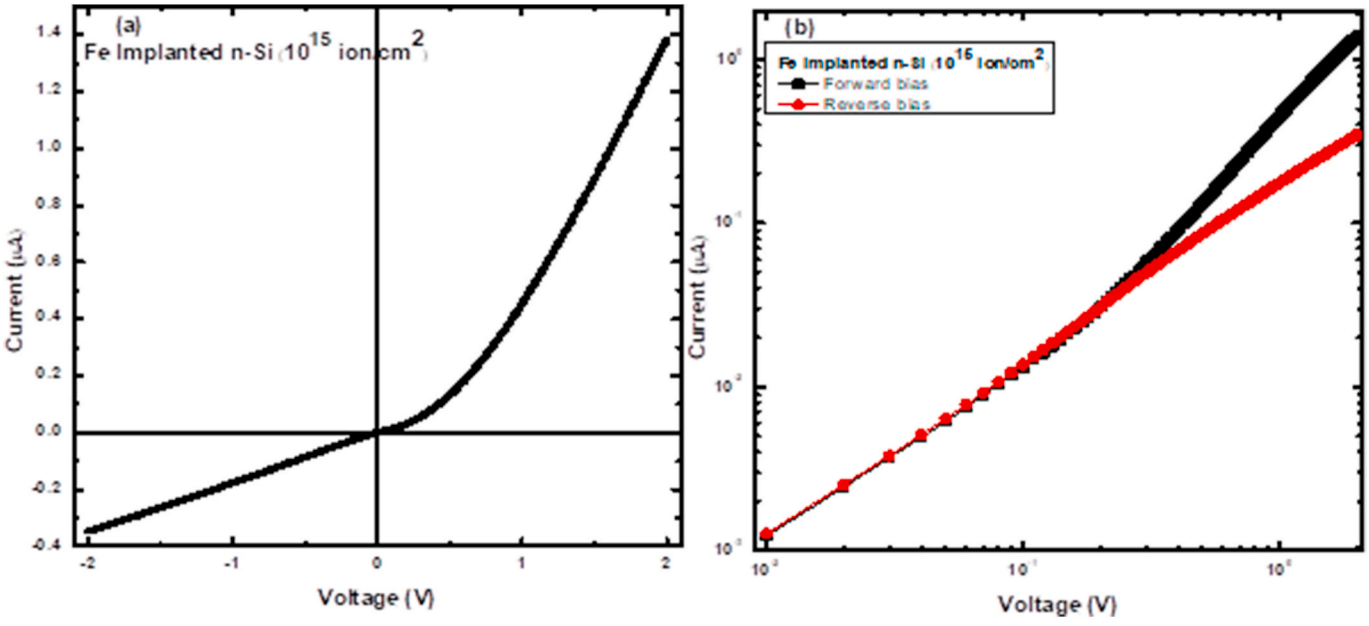

Fig. 3. I–V characteristics of the diode fabricated on Fe-implanted *n*-Si in linear-linear (a) and in logarithmic (b) scales. The Si substrate was implanted to the fluence of 10^{15} ion/cm^2.

that at this position it is not affected by incident particle [22]. *g-r* centres are responsible for ohmic behaviour of the diode, as shown in the figure. In this case the Fermi energy is pinned at intrinsic position and the material becomes intrinsic-like [11].

An ohmic behaviour was also observed on the diodes that were fabricated on Au-doped *n*-Si [21] and Pt-doped *p*-Si [5]. Thus, in Si, Fe exhibits properties that are similar to Au and Pt. Fig. 3(b) also shows that the forward current is higher than the reverse current at voltages higher than 0.32 indicating that the density of Fe-induced *g-r* defect centres is not enough at this fluence for the trends to be ohmic for the whole voltage range. At this high voltage range, $g < r$.

Fig. 4(a) shows *I–V* characteristics of the diode fabricated on *n*-Si implanted by Fe to a fluence of 10^{16} ion/cm^2. The reverse current is independent of the voltage at the range of 0 V to −0.4 V and starts to vary with voltage from −0.41 to −2 V on the reverse bias. Unlike in the case of the unimplanted Si-based diode in Fig. 2(a), the current has increased at high voltages for this diode.

Fig. 4(b) shows that reverse current and forward current trends are the same for the whole voltage range indicating that the density of Fe-induced g-*r* centres has increased. It can be seen from Fig. 4(b) that the ohmic region has increased to show that for this diode $g = r$ for the whole voltage range. Similar *I–V* behaviour was observed on commercial Si diodes that were heavily irradiated by 1 MeV neutron [12]. The ohmic region, a region where forward current is the same as reverse current, was found to increase with radiation fluence [11,12]. The diodes that showed a high ohmic region were found to be more resistant to radiation damage and were described in terms of a high concentration of defect levels positioned at the centres of the energy gap [12]. A tendency of reverse current to saturate is not observed in Fig. 4(b). The suppression of saturation indicates a typical behaviour of diodes fabricated on the material that has a high density of *g-r* centres [11,12]. Thus, doping with Fe is similar to heavy neutron irradiation of Si, both induce *g-r* centres that are responsible for ohmic *I–V* behaviour of the material-based diodes.

Fig. 5(a) shows *I–V* characteristics of the diode fabricated on *n*-Si implanted by Fe to a fluence of 10^{17} ion/cm^2 in a linear-linear scale. The reverse current has increased and varies linearly with voltage for the whole voltage range. This increase indicates that the density of charge carriers withdrawn to the opposite electrodes to contribute to the measured current has increased for this diode. The forward current, too, has increased and it varies linearly with voltage.

The trends in Fig. 5(b) show that the reverse current becomes completely ohmic and not showing any tendency of saturation in a logarithmic scale. Similarly, the forward current exhibits an ohmic characteristics which tends to increase the slope at 0.34 V. The forward and reverse currents are the same at low voltage range of 0.01–0.33 V indicating that a charge distribution mechanism in the material is dominated by *g-r* centres at this voltage range. Since the density of defect levels at the centre of energy gap (*g-r* centres) increases with fluences [11,12,21], it was expected that the linear region would be observed for the whole voltage range for this diode. This discrepancy of the results is explained later in the text.

The quality of the fabricated diodes and a change in *I–V* properties of the diodes with an increase in Fe fluence is explained by comparing the trends in logarithmic scales for all diodes. This comparison is presented in Fig. 6. The quality of the diodes can be explained by rectification ratio, a ratio of the forward current to the reverse current at 2 V. The ratio for unimplanted *n*-Si based-diode was evaluated to be 1.63×10^4. This high rectification ratio is due to the huge difference between the reverse and forward currents at 2 V and it is within the acceptable range in comparison to those obtained in the literature [23,24] indicating that the diodes were well fabricated.

In comparing trends for the unimplanted *n*-Si - based diode in Fig. 6 (a) with those of the diode fabricated on Fe-implanted to 10^{15} ion/cm^2 in Fig. 6 (b), it can be seen that for the trends in Fig. 6 (b) to be ohmic, close to each other, the forward current has decreased by a factor 4 while the reverse has increased by a factor 10^3. A high increase in reverse current indicates more holes (minority carrier) have been created in the material after Fe implantation to this fluence. Thus, in addition to *g-r* centres to induce ohmic behaviour, Fe also introduces acceptor levels in the energy gap of Si. It is possible that in Si, Fe also introduces donor levels in the energy gap since the forward current has increased at low voltages. Relative to other levels, the density of the induced donor levels is low, and electrons generated by these levels are quickly recombined with holes resulting in a reduction of forward current at high voltages.

A rectification ratio for diode fabricated on the material implanted to 10^{15} ion/cm^2 was evaluated to be 4. This low rectification ratio is due to defects that have been induced by Fe in Si and not metal-semiconductor (*m-s*) interface nor any surface-related defects. If a change in *I–V* trends were due to interface property, an ohmic behaviour would have been

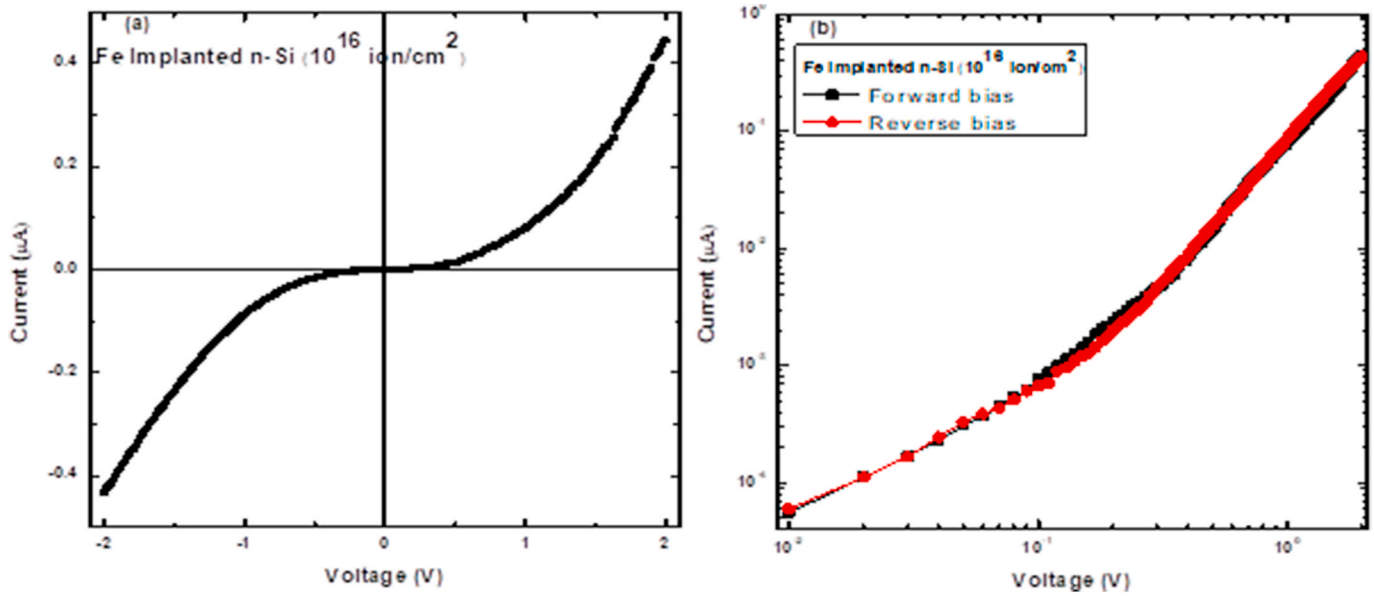

Fig. 4. I–V characteristics of the diode fabricated on Fe-implanted *n*-Si in linear-linear (a) and in logarithmic (b) scales. The Si substrate was implanted to the fluence of 10^{16} ion/cm^2.

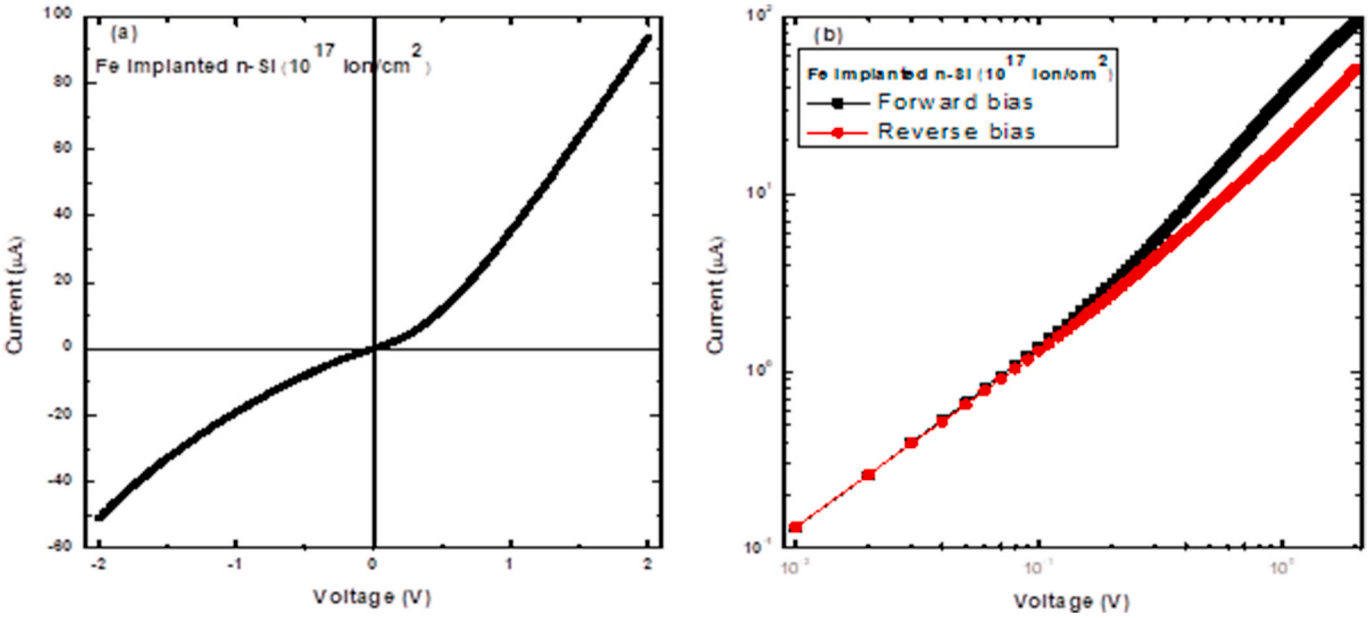

Fig. 5. I–V characteristics of the diode fabricated on Fe-implanted *n*-Si in linear-linear (a) and in logarithmic (b) scales. The Si substrate was implanted to the fluence of 10^{17} ion/cm^2.

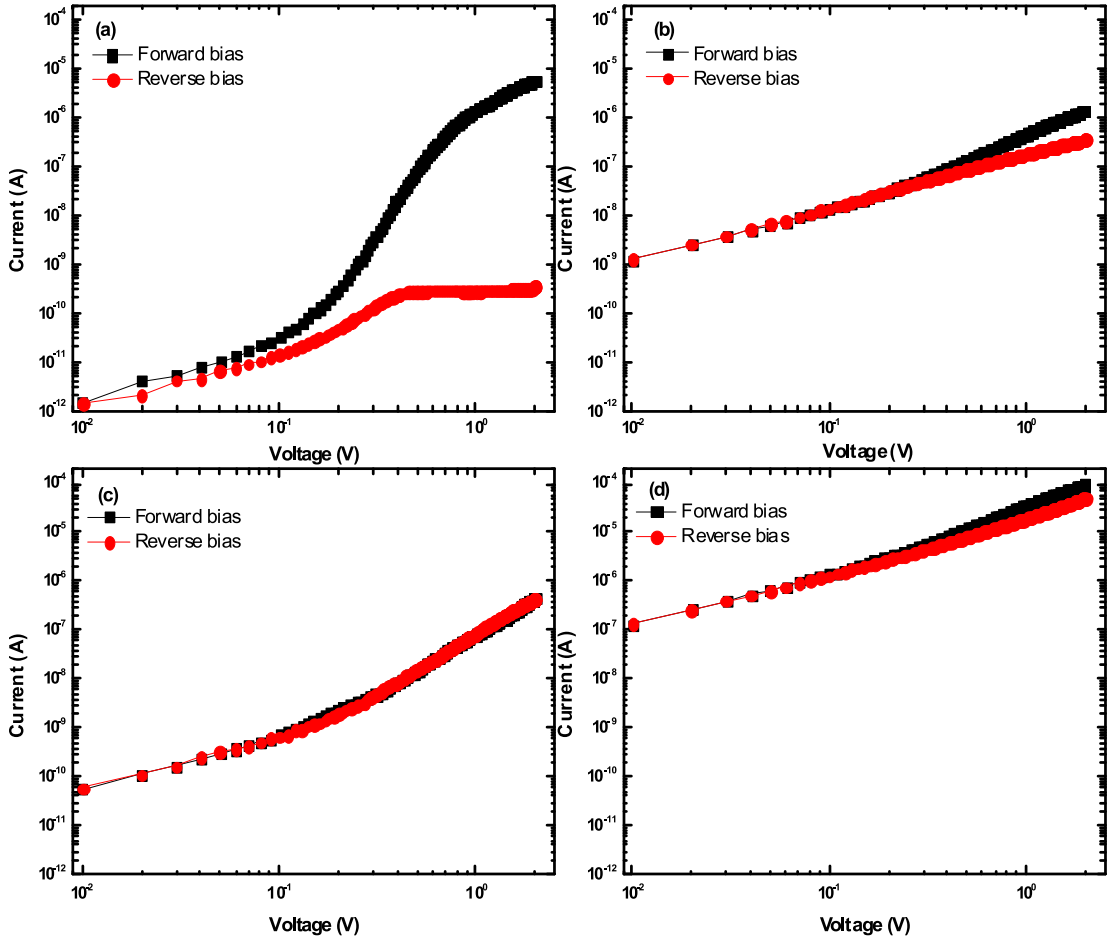

Fig. 6. I–V characteristics of the diodes fabricated on unimplanted *n*-Si (a), Fe-implanted *n*- Si to the fluence of 10^{15} (b) 10^{16} (c) and 10^{17} ion/cm^2 (d) in logarithmic scales.

observed in Fig. 5 (a) since the diodes were fabricated in the same conditions. It is therefore, argued here that the diodes were well fabricated and a change in *I–V* properties is due to defects that were induced by Fe in Si. The confusion here is that equation (1) describes *I–V* properties of the diodes that are fabricated on lifetime (*g-r* defect-free) material and it is inadequate to describe the behaviour of the diode when a charge distribution mechanism in the material involves that of *g-r* centres.

As the density of *g-r* centres increases to increase the ohmic region of the device, it can be seen in Fig. 6 (c) that the forward current has decreased by a factor of 16 and reverse current increased by a factor of 1.3×10^3 in comparison to the currents in Fig. 6 (a) at 2 V. This variation of currents indicates that more holes (acceptor levels) are generated (introduced) in the material as Fe fluence increases. This introduction of acceptor levels results in a rectification ratio of 1.0 showing a complete ohmic behaviour of the diode. A ratio of unity and the results presented in Fig. 6 (c) confirm that for this diode a charge distribution mechanism in Si is completely dominated by *g-r* centres.

Trends in Fig. 6 (d) are very close to each and they are higher than trends of other diodes indicating that the conductivity (resistivity) has increased (decreased) for the diode fabricated on the material implanted with Fe to the highest fluence, 10^{17} ion/cm^2. In comparison to currents in Fig. 6 (a) the current has increased by a factor of 16.5 and 1.3×10^3 for forward and reverse, respectively. Though they are very close to each other, the forward current is slightly higher than the reverse current at 2 V with the rectification ratio of 1.84.

The variation of diode rectification ratio has been used to further investigate a change in diode *I–V* properties with Fe fluence and it is shown in Fig. 7. A decrease in rectification ratio is observed up to the fluence of 10^{16} ion/cm^2 and then increases gently with fluence. According to Ref. [24] a decrease in rectification ratio is due to a decrease (increase) in the density of majority (minority) charge carriers. This variation of the density implies that in *n*-Si electrons are compensated or recombined with Fe-introduced acceptor levels to increase the resistivity of the material. This increase in resistivity is confirmed by high R_S evaluated on this diode (shown later in the text).

At the fluence, 10^{16} ion/cm^2, where the intensity of acceptor and donor levels are equal, the material exhibits intrinsic-like behaviour and its conductivity (resistivity) is at minimum (maximum) [11]. This work shows that when the conductivity of Si is at minimum a device fabricated on the material is completely ohmic with a rectification ratio of 1.0. With increase Fe implantation fluence the rectification ratio increases gently with fluence. This increase indicates that the conductivity of the material is dominated by holes at high voltages. A deviation of forward current from reverse current in Fig. 6 (d) is as a result of holes dominating material conductivity at high voltage range.

The slope with which the rectification ratio changes before the implantation fluence of 10^{16} ion/cm^2 is higher than the slope after the implantation fluence of 10^{16} ion/cm^2, though Fe is implanted at the same rate in Fig. 7. A difference in slopes indicates that a charge carrier distribution mechanism is not due to only donor and acceptor levels but also *g-r* centres in Si. This involvement of *g-r* centres in the conduction mechanism was observed by ohmic behaviour of the devices after Fe implantation.

The results presented in Fig. 7 shows that the conductivity of *n*-Si has been inverted from *n*- to *p*-Si. The difference in slopes in Fig. 7 also indicates that hole generation rate is higher before the conductivity-type inversion. A conductivity-type inversion of Si was reported based on the material that was irradiated by 1 MeV neutrons and was found to occur at the neutron fluence of 1.4×10^{13} n/cm^2 [25–27]. The fluence where the conductivity-type inversion occurred for Fe-doping is higher in this work because in Si neutrons are more damaging. A conductivity-type inversion was also reported based on the data acquired from on Au-doped-silicon-based diode [28]. Thus, in Si, Fe exhibits similar properties as neutron radiation and Au.

Semi-logarithmic plots of the current trends were produced to further investigate a change in *I–V* characteristics of the diodes with implanted Fe fluence. The plots are shown in Fig. 8. The ideality factor, which is the measure of diode quality and other diode parameters were evaluated using the slope of the linear region in forward bias as

$$\eta = \frac{q}{kT}\frac{\mathrm{d}V}{\mathrm{dln}(I)}. \tag{2}$$

The saturation current,

$$I_s = AA^{**}T^2 \exp\left(\frac{-q\varphi_b}{kT}\right) \tag{3}$$

was calculated from the intercept on the *y*-axis of the plots. The Schottky barrier height , φ_b, on the other hand, was calculated by substituting the value of I_s in equation (3). In the above equation, A (=2.83×10^{-3} cm^2) is the diode active area and A^{**} (= 112 A cm^{-2} K^{-2}) is the effective Richardson constant for *n*-type silicon.

The forward bias *I–V* trend of the diode fabricated on unimplanted *n*-Si is linear on a semi-logarithmic scale at low voltages, but deviate significantly from linearity due to the effect of series resistance (*Rs*) [28], the interfacial insulator layer [19] and the interface states [29] when the applied voltage is large. The ideality factor evaluated from

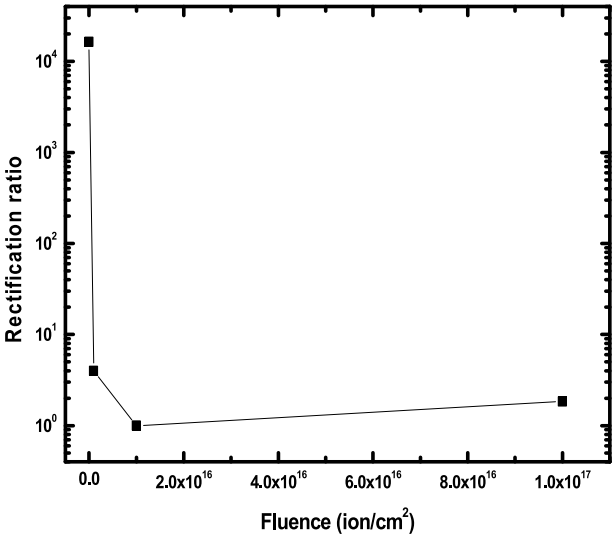

Fig. 7. Variation of rectification ratio with iron fluence.

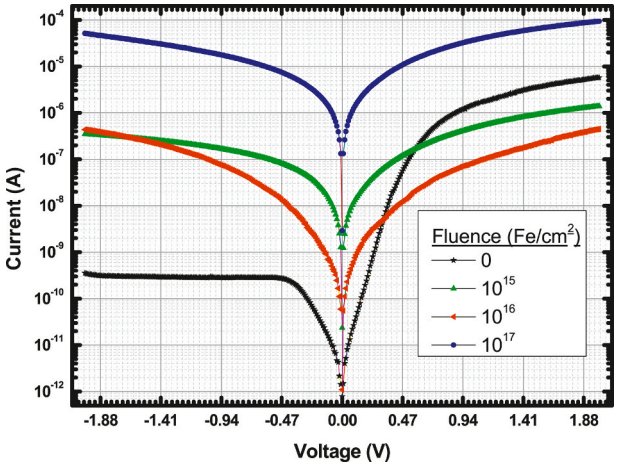

Fig. 8. Forward and reverse bias semi-logarithmic I–V characteristics of Schottky diodes fabricated on unimplanted and iron-implanted n-Si to different fluences.

unimplanted n-Si-based diode is, 1.79, higher than unity to show that the diodes *I–V* behaviour has deviated from ideal thermionic emission mechanism [28]. This ideality factor is, however, close to 1.62 reported based on the *n*-4H–SiC diode fabricated using palladium for Schottky contact [30] and lower than 2.898 evaluated on Au/SiO_2/*n*-Si diodes [31]. Though the ideality factor evaluated in this work indicates that the diode is non-ideal, it falls within the range of those reported before and the results presented in Fig. 8 indicating the rectifying behaviour.

The high value of the ideality factor attests that there are different conduction mechanisms contributing to the measured forward current of the diode other than thermionic emission. In addition to thermionic emission mechanism, the forward current of the diode fabricated on unimplanted n-Si-based diode in Fig. 8 is probably also due to the tunnelling mechanism making the total diode current in equation (1) modified to

$$I_{TOT} = I_{TE} + I_{TU} \tag{4}$$

where I_{TE} and I_{TU} are currents due thermionic emission and tunnelling mechanisms, respectively, given [32] as

$$I_{TE} = I_S \left[\exp\left(\frac{qV - IR_S}{\eta kT}\right) - 1\right] \tag{5}$$

and

$$I_{TU} = I_{TU(0)} \left[\exp\left(\frac{qV - IR_S}{E_0}\right) - 1\right] \tag{6}$$

In equation (6), $I_{TU(0)}$ is the tunnelling saturation current and E_0 is the tunnelling parameter defined as

$$E_0 = E_{00} \coth\frac{E_{00}}{kT} \tag{7}$$

where the characteristic tunnelling energy, E_{00}, is given in terms of the doping density, *N*, and the silicon dielectric constant , ε, as

$$E_{00} = \left(\frac{qk}{4\pi}\right)\left(\frac{N}{m^*\varepsilon}\right) \tag{8}$$

This tunnelling conduction mechanism is probably due to SiO_2 layer formed between Au and Si resulting in a recombination of charge carriers through the interface states [33].

The forward current trends for Fe-implanted n-Si-based diodes presented in Fig. 8 are different from that of unimplanted n-Si-based diode indicating the involvement of additional conduction mechanism in the diode current. As discussed before, using Figs. 2–6, the additional current component is due generation-recombination centres that were induced by Fe in the energy gap of silicon making the total current be

$$I = I_{TE} + I_{TU} + I_{GR} \tag{10}$$

where I_{GR} is the current due to generation-recombination mechanism given [34] as

$$I_{GR} = I_{GR(0)} \left[\exp\left(\frac{qV - IR_S}{\eta kT}\right) - 1\right] \tag{11}$$

The recombination activity of generation-recombination conduction mechanism is observed in forward bias and it is expressed [35] as

$$I_R = I_{R(0)} \exp\left(\frac{qV - IR_S}{\eta kT}\right)\left[1 - \exp\left(\frac{-qV + IR_S}{kT}\right)\right] \tag{12}$$

where $I_{R(0)}$ can be presented in terms of the intrinsic carrier concertation, n_i, the width of the depletion region, *w,* and the recombination lifetime, τ_r, [32] as

$$I_{R(0)} = \frac{qn_i w}{2\tau_r} \tag{13}$$

It can be noticed in Fig. 8 that generation-recombination conduction mechanism dominates at low voltage range up to 0.55 V and 0.32 V for the diodes fabricated on Fe-implanted *n*-Si to 10^{15} Fe/cm^2 and 10^{16} Fe/cm^2, respectively. The forward current trend for 10^{16} Fe/cm^2 is lower than that of 10^{15} Fe/cm^2 showing that carrier compensation is higher due to the generation and recombination rates being the same to increase the resistivity of the material. For the diode fabricated on Fe-implanted *n*-Si to 10^{17} Fe/cm^2, on the other hand, the mechanism dominates for the whole voltage range indicating that the density of *g-r* centres has increased. At the highest fluence, the density of the induced defects in Si bulk is so high and more dominating the conduction mechanisms such that interfacial insulator layer and the interface states surface effects on *I–V* characteristics are negligible.

The ln*I- V* plots of the diodes fabricated on Fe-implanted n-Si do not show a clear linear making it difficult to evaluate parameters for these diodes. The ln*I-V* method is, therefore, unsuitable to explain parameters of the diode fabricated on *g-r* centre defected material. The most common and reliable method to evaluate the parameters is Cheung's method. In this method the forward diode current is related to R_S [36] as

$$\frac{dV}{d(\ln I)} = \left(\frac{\eta kT}{q}\right) + IR_s \tag{14}$$

$$H(I) = V - \left(\frac{\eta kT}{q}\right)\ln\left(\frac{I}{AA^*T^2}\right) \tag{15}$$

and $H(I)$ is given as

$$H(I) = \eta\varphi_b + IR_s. \tag{16}$$

Equations (14)–(16) show that the plots of $\frac{dV}{d(\ln I)}$ and $H(I)$ - *I* would be linear with the slopes of the plots being R_s. η and φ_b are obtained from the *y*-axis intercepts of $\frac{dV}{d(\ln I)}$ and $H(I)$ -*I*, respectively. The linear plots were generated (not shown) and parameters evaluated are presented in Table 1.

Values of ideality factor and Schottky barrier height evaluated using different methods are due to the existence of R_s [37] and possibly due to different linear regions parameters are evaluated from. For ln(*I*) – *V* method, parameters are evaluated based on the current measured at low-voltage ranges only where the effects of R_s are minimal. Ideality factors evaluated on unimplanted *n*-Si based diode using both methods are relatively close to each other with the one obtained using d*V*/d ln (*I*) – *I* method being 0.12 higher.

A very big difference in ideality factors using both methods for the same Fe implanted *n*-Si based diodes further attests the unsuitability of ln(*I*) – *V* method to evaluate parameters when the conduction mechanism involves charge generation/recombination in the material. The ideality factor using ln(*I*) – *V* method are much higher possibly since in this method they are evaluated at a region below the silicon surface than on the whole space charge region.

It is interesting to see that the value of the ideality factor for the diode fabricated on *n*-Si implanted to the highest fluence is 1.00 though the *I–V* trends indicate that other diode conduction mechanisms are involved other than thermionic emission. The ideality factor of 1.00 evaluated for this diode probably indicates that the parameter is less dependent on the defects induced in the material hence less pronounced when the diode conduction mechanism is completely dominated by

Table 1
The electrical parameters of unimplanted and Fe-Implanted silicon to different fluences calculated with different methods.

Fluence (Fe/cm^2)	ln*I-V*			d*V*/dln *I–I*		*H (I) – I*	
	η	φ_B	I_s (nA)	η	R_s(k Ω)	φ_B	R_s(k Ω)
0	1.79	0.94	0.003	1.91	20.0	0.95	231.0
10^{15}	5.19	0.75	5.330	1.32	83.0	0.92	1260
10^{16}	4.32	0.84	0.171	2.58	157	0.91	3620
10^{17}	5.08	0.63	580.0	1.00	2.00	0.80	20.00

charge carrier distribution in the bulk. In the case of the diode fabricated on *n*-Si implanted to the highest fluence R_S is low due to the high density of charge carrier density generated by *g-r* centres to the space charge region, hence the high evaluated saturation current. A high saturation current corresponds to low Schottky barrier height indicating high charge carrier density through the region can be achieved with low energy.

Values of series resistance evaluated using dV/dln I–I and $H(I) - I$ are different for all diodes and the explanation of this difference is currently not known. The variation R_s evaluated from both methods with fluence is, however, the same. It can be seen from the table that the highest R_s is evaluated for the diode fabricated on *n*-Si implanted to the fluence of 10^{16} Fe/cm^2. This high R_s for this diode indicates that the resistivity of the material is at maximum at the point of conductivity-type inversion. $g = r$ at this point, resulting in the ohmic I–V behavior of the material-based device.

4. Conclusion

In this work, Schottky diodes were well fabricated on undoped and Fe-implanted *n*-Si. The diodes were characterized using the I–V technique. Diodes that were fabricated on Fe-implanted *n*-Si show ohmic I–V behaviour. This ohmic behaviour indicated that in Si, Fe induce *g-r* centres, defect levels positioned at the centre of the energy gap. The observed increase in ohmic region indicated that the induced *g-r* centres increased with fluence. In addition, the obtained results indicated that in Si, Fe was responsible for a change in conductivity-type of the material from *n*-to *p*-type. At the point of conductivity-type inversion the resistivity of the material is at maximum and the trends are ohmic for the whole voltage range. Furthermore, a change in diode parameters with Fe implantation was studied in this work. Properties of diodes fabricated on Fe-implanted Si were similar to those of the diodes that are resistant to radiation damage. In conclusion, Fe is a promising dopant in a search to improve radiation-hardness of Si to be used in high energy physics experiments. Fe can then compete with already proposed metals, Au and Pt, and heavy irradiation in tuning Si properties to be suitable for the application.

Author statement

J. O. Bodunrin: student investigator, data analysis, original draft preparation.

D. A. Oeba: editing.

S. J. Moloi: supervision, conceptualization, methodology, writing-reviewing and editing.

Declaration of competing interest

The authors declare that they have no known competing financial interests or personal relationships that could have appeared to influence the work reported in this paper.

Acknowledgement

The first author acknowledges the National Research Foundation (NRF) and The World Academy of Science (TWAS) for student funding (Grant number 116113). This work is based on the research supported wholly by the National Research Foundation of South Africa (Grant numbers 105292 and 114800). We would like to thank Mr. Tony Miller of iThemba LABS for Iron implantation.

References

[1] G. Kramberger, Nucl. Instrum. Methods A 924 (2019) 192.
[2] P.G. Litovchenko, A.A. Groza, V.F. Lastovetsky, L.I. Barabash, M. I Starchik, V. K. Dubovoy, et al., Nucl. Instrum. Methods A 58 (2006) 78.
[3] L. Fonseca, et al., Microelectron. Reliab. 40 (2000) 791.
[4] R.L. Dixon, K.E. Ekstrand, Radiat. Protect. Dosim. 17 (1986) 527.
[5] S.J. Moloi, M. McPherson, Physica B: Phys. Condens. Matter 404 (2009) 2251.
[6] C.B. Collins, R.O. Carlson, Phys. Rev. 108 (1957) 1409.
[7] J.D. Gerson, L.J. Cheng, J.W. Corbett, J. Appl. Phys. 48 (1977) 4821.
[8] H.R. Szawelska, H. Feichtinger, J. Phys. C Solid State Phys. 14 (1981) 4131.
[9] K. Watanabe, C. Munakata, Semicond. Sci. Technol. 8 (1993) 230.
[10] Y.K. Kwon, T. Ishikawa, H. Kuwano, J. Appl. Phys. 61 (1987) 1055.
[11] B.K. Jones, M. McPherson, Semicond. Sci. Technol. 14 (1999) 667.
[12] S.J. Moloi, M. McPherson, Physica B: Phys. Condens. Matter 404 (2009) 3922.
[13] S. Mahato, J. Puigdollers, Physica B: Phys. Condens. Matter 530 (2018) 327.
[14] M. Siad, A. Keffous, S. Mamma, Y. Belkacem, H. Menari, Appl. Surf. Sci. 236 (2004) 366.
[15] S.M. Sze, Physics of Semiconductor Devices, second ed., Wiley, New York, 1981.
[16] B.G. Streetman, Solid State Electronic Devices, third ed., Prentice Hall, London, 1990.
[17] D.K. Schroder, Semiconductor Material and Device Characterization, third ed., Wiley, New York, 2006.
[18] S. Agarwal, M. Seetharaman, N.K. Kumawat, A.S. Subbiah, S.K. Sarkar, D. Kabra, M.A. Namboothiry, P.R. Nair, J. Phys Chem Lett. 5 (2014) 4115.
[19] O. Gullu, S. Aydogan, A. Turut, Microelectron. Eng. 85 (2008) 1647.
[20] S. Aydogan, O. Gullu, A. Turut, Mater. Sci. Semicond. Process. 11 (2008) 53.
[21] M. Msimanga, M. McPherson, C. Theron, Radiat. Phys. Chem. 71 (2004) 733.
[22] V.N. Brudnyi, S.N. Grinyaev, V.E. Stepanov, Physica B: Phys. Condens. Matter 212 (1995) 429.
[23] N.G. Park, et al., Unconventional Thin Film Photovoltaics, Royal Society of Chemistry, 2016.
[24] M.J. Parida, S.T. Sundari, V. Sathiamoorthy, S. Sivakumar, Nucl. Instrum. Methods A 905 (2018) 129.
[25] L. Agarwal, B.K. Singh, S. Tripathi, P. Chakrabarti, Thim Solid Films 612 (2016) 259.
[26] I.M. Afandiyeva, S. Demirezen, S. Altındal, J. Alloys Compd. 552 (2013) 423.
[27] D. Pitzl, N. Cartiglia, B. Hubbard, D. Hutchinson, J. Leslie, K. O'Shaughnessy, et al., Nucl. Instrum. Methods A 311 (1992) 98.
[28] S. Aydogan, M. Saglam, A. Turut, Microelectron. Eng. 85 (2008) 278.
[29] R.T. Tung, Phys. Rev. B 64 (2001) 205.
[30] S. Krishnana, D. Sanjeev, M. Pattabi, Nucl. Instrum. Methods B 266 (2008) 621.
[31] H. Altuntaş, S. Altındal, H. Shtrikman, S. Ozçelik, Microelectron. Reliab. 49 (2009) 904.
[32] S. Amor, et al., *012001*, Conf. Ser.: Mater. Sci. Eng. 186 (2017).
[33] Q.K. Yang, F. Fuchs, J. Schmitz, W. Pletschen, Appl. Phys. Lett. 81 (2002) 4757.
[34] S.M. Sze, K.K. Ng, Physics of Semiconductor Devices, John wiley & sons, 2006.
[35] S. Mohammad, H. Morkoc, Prog. Quant. Electron. 20 (1996) 361.
[36] S.K. Cheung, N.W. Cheung, Appl. Phys. Lett. 49 (1986) 85.
[37] T. Kilicoglu, Thin Solid Films 516 (2008) 967.